ERDC/EL MP-21-1

US Army Corps
of Engineers®
Engineer Research and
Development Center

ERDC
ENGINEER RESEARCH & DEVELOPMENT CENTER

Computational Investigation on Interactions Between Some Munitions Compounds and Humic Substances

Timothy C. Schutt and Manoj K. Shukla

February 2021

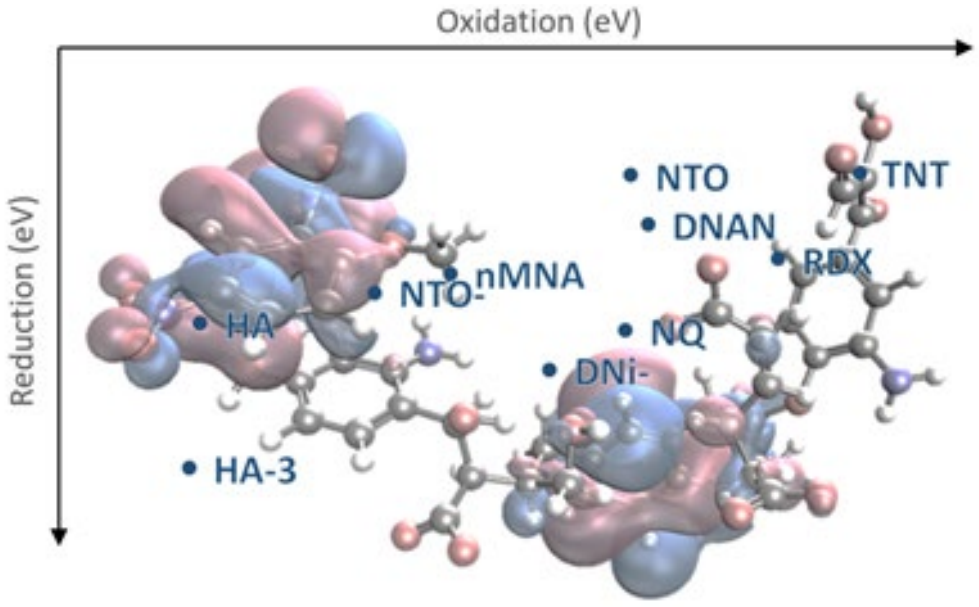

Environmental Laboratory

The U.S. Army Engineer Research and Development Center (ERDC) solves the nation's toughest engineering and environmental challenges. ERDC develops innovative solutions in civil and military engineering, geospatial sciences, water resources, and environmental sciences for the Army, the Department of Defense, civilian agencies, and our nation's public good. Find out more at www.erdc.usace.army.mil.

To search for other technical reports published by ERDC, visit the ERDC online library at https://erdclibrary.on.worldcat.org/discovery.

ERDC/ELMP-21-1
February 2021

Computational Investigation on Interactions Between Some Munitions Compounds and Humic Substances

Timothy C. Schutt and Manoj K. Shukla

Environmental Laboratory
U.S. Army Engineer Research and Development Center
3909 Halls Ferry Road
Vicksburg, MS 39180-6199

Final report

Prepared for US Army Corps of Engineers
Washington, DC 20314

Under Project Number 03E, Program Element 63728

Abstract

Humic acid substances (HAs) in natural soil and sediment environments effect the retention and degradation of insensitive munitions compounds and legacy high explosives (MCs): DNAN, DNi- NH_4^+, nMNA, NQ, NTO (neutral and anionic forms), TNT, and RDX. A humic acid model compound has been considered using molecular dynamics, thermodynamic integration, and density functional theory to characterize the munition binding ability, ionization potential, and electron affinity compared to that in the water solution. Humic acids bind most compounds and act as both a sink and source for electrons. Ionization potentials suggest HAs are more susceptible to oxidation than the MCs studied. The electron affinity of HAs are very conformation-dependent and spans the same range as the munition compounds. When HAs and MCs are complexed the HAs tend to radicalize first thus buffering MCs against reductive as well as oxidative attacks.

Contents

Abstract ii

Figures and Tables iv

Preface v

1 Introduction 1

2 Computational Methods 3

2.1 Molecular Dynamics (MD) setup 3

2.2 MD-Docking/Structure Generation 6

2.3 Thermodynamic Integration (TI) 6

2.4 Density Functional Theory (DFT) 7

3 Results and Discussion 9

3.1 Hydrogen Bonding 9

3.2 Binding Between Munition and Humic Substances 10

3.3 Ionization Potentials (IP) and Electron Affinities (EA) 12

4 Conclusions 18

Abbreviations 19

References 21

Report Documentation Page

Figures and Tables

Figures

Figure 1. Diagram of the humic acid model, HA, used to capture main functional groups known to be in humic substance in a relatively small number of atoms. HA^{-3} is a tri-anionic form of HA where carboxylic acid groups (arrows) are deprotonated. 3

Figure 2. Defined structures for the munition compounds included in study. Acronym definitions for the munition compounds are as follows: DNAN – 2,4-Dinitroanisole; NH4+DNi -- Ammonium Dinitramide; TNT – 2,4,6-Trinitrotoluene; NQ -- 1-Nitroguanidine; nMNA – N-methyl-p-nitroaniline; RDX -- 1,3,5-Trinitro-1,3,5-triazinane; NTO – 3-nitro-1,2,4-triazol-5-one (neutral form); NTO- – conjugate base of NTO (anionic/deprotonated form)..... 5

Figure 3. The redox (bottom rectangle) and EA/IP (top rectangle) properties of isolated MC and HA compounds..... 14

Figure 4. HOMO and LUMO orbital densities for TNT-HA^{-3} complex. The HOMO is localized on the aldehyde end of HA (left side) and the LUMO is localized on TNT (top left). 16

Tables

Table 1. Average number of hydrogen bonds in between species-pairs at any particular snapshot in the MC-HA bound complexes in water solution. The species pairs are represented in the form of MC/Water, HA/Water, HA/MC and HA/HA pairs where HA/HA pair is due to the formation of intramolecular hydrogen bonds..... 10

Table 2. Average Gibbs free binding energies of munition to HA from thermodynamic integration (TI) in kcal/mol. Standard deviations are about 1.7 kcal/mol for each system..... 11

Table 3. The BSSE-corrected binding energies (kcal/mol) for the lowest energy configuration of munition compounds with humic acid (neutral and tri-anionic forms) complexes calculated at CPCM/M06-2X/6-311G(d,p) level..... 12

Table 4. Ionization potential (IP), electron affinity (EA), oxidation and reduction potentials for each of the complexed munition-humic systems with CPCM implicit solvent at M06-2X/6-311G(d,p) level. All energies are in eV..... 14

Table 5. Ionization potential (IP), electron affinity (EA), oxidation and reduction potentials for each of the conformations of HA individually with CPCM implicit solvent at M06-2X/6-311G(d,p) level. All energies are in eV..... 16

Preface

This study was conducted for the US Army Corps of Engineers, Engineer Research and Development Center (USACE-ERDC) under the USACE Environmental Quality Technology Program and the Department of Defense (DoD) Environmental Security Technology Certification Program (ESTCP), Project 03E, Program Element Number 63728, Task 01. The technical monitor was Elizabeth Ferguson.

The work was performed by the Environmental Processes Chemistry Branch (EPC) of the Environmental Processes Division, U.S. Army Engineer Research and Development Center, Environmental Laboratory (ERDC-EL). At the time of publication, Amber Russell was Branch Chief; Warren Lorentz was Division Chief; and Elizabeth Ferguson was the Technical Director for Installation and Operation Environment (IOE). The Deputy Director of ERDC-EL was Dr. Jack Davis and the Director was Dr. Edmund Russo.

This paper was originally published in the *Journal of Physical Chemistry A* on 14 December 2020.

The Commander of ERDC was COL Teresa A. Schlosser and the Director was Dr. David W. Pittman.

1 Introduction

The fate and transport of compounds in environmental media remains a difficult problem to predict for environmental impact models.[1] This challenge is largely due to the complex heterogeneity of soils and convoluting factors such as vegetation and weather that make it very difficult to generalize the modeling involving soils.[1,2] A key component of the soils that is responsible for a significant part of the binding and electronic interaction with solutes is humic acid substances (HAs).[3,4,5] A common definition of HAs is "that portion of 'humus' which is soluble in sodium hydroxide solution and precipitated by acidification of the alkaline extract."[6] More generally, HAs are organic matter in soils from both plant and animal sources subjected to various stages of decomposition/recombination.[6] HAs are very diverse in structure as well as function within an ecosystem.[7] Structural characterization of HAs has revealed a polycyclic aromatic core with attached polysaccharides, proteins, relatively simple phenols, and metals.[8,9] Analyzing such materials requires multiple characterization methods[7] and diverse research approaches to elucidate the prominent structures,[10–16] resulting in significant effort and cost burden. Computational models capable of accurately predicting the interactions of different aspects of HAs, and similarly fulvic acids,[17] have the potential to reduce characterization costs by enabling accurate extrapolation from existing experimental HA-sorption data to sorbates that are untested and/or that are difficult to test safely, such as munition compounds and chemical warfare agents.

Some amounts of munition compounds (MCs) could be released into local environments surrounding testing ranges, training sites, manufacturing, and storage locations.[18] It is important to understand the distribution, degradation, and impact these MCs will have in order to evaluate the potential effects on local ecosystems.[19–21] HAs play a large role in the abiotic component of binding and degradation of MCs observed in soil samples.[4,5] HAs can bind the MCs very strongly, with K_{OC} values as much as 2 orders of magnitude higher than whole soils.[5] HAs can also catalyze their degradation, form radical species, and change function based on pH.[6,12,14,22–26] In their review of research on humic substances, Sutton *et. al.*[11] pointed out the need for computational elucidation of the intermolecular interactions (e.g. H-bonding, hydrophobic, π-stacking, etc.) and the collective

strength and endurance of those interactions which govern the behavior of humic materials. The works of Mark *et. al.*[27,28] on NTO binding in soils reveal that organic content dramatically impacts the compounds fate and transport properties and has a strong dependence on pH. Additionally, the experimental results of Martin *et. al.*[29] on the binding of oxyanions with humic substances probe ternary complexation and conclude that charge neutralization alone is insufficient to explain the binding mechanism. Martin *et. al.* conclude that fundamental coordination chemistry is critical for fate and transport modeling of compounds within humic-rich environments.[29] This study seeks to build towards meeting this need by simulating the interactions of a model HA structure with various MCs and evaluating changes in the binding energies, redox properties, electron affinities, and ionization potentials of the complexes. This data illustrates the various interactions, mechanisms, and some impacts of how HAs affect fate and transport of MCs in the environment. The data shows that HAs can buffer MCs against both oxidative and reductive degradation mechanisms potentially increasing the persistence of MCs in natural environments.

2 Computational Methods

2.1 Molecular Dynamics (MD) setup

MD simulations were carried out in the Amber16 software package.[30] The MC and HA forcefields were based on GAFF parameters[31,32] for the bond, angle, dihedral, and van der Waals terms while the point charges were calculated with the restrained electrostatic potential (RESP) method as implemented in antechamber.[33] The MP2 level of theory[34] and the cc-pVTZ basis set[35] as implemented in Gaussian16[36] were used to calculate the electrostatic potential derived charges according to the Merz-Singh-Kollman scheme (MK charges) as the input to the antechamber RESP method.[33] The best-fit point charges were not scaled down by the 80% factor that is typically applied[31,37] to charges calculated at HF/6-31g level, as recent studies have shown good reproduction of dynamic properties of simple organic and ionic molecules when using RESP charges calculated at the MP2/cc-pVTZ level.[38–40] Water molecules were defined by the TIP3P model and the GAFF ion forcefield files were chosen to match the water selection.[41]

The model HA structure[42] was developed based on the TNB humic acid building block by Sein *et. al.*[43] with the minor modification of cyclization of the benzyl keytone oxygen to form a heterocyclic ring. The TNB humic acid building block incorporates the results of experimental data and retro-biosynthetic analyses of humic substances. Newer humic acid models such as those used by Lan *et. al.*[44] and Petrov *et. al.*[45] incorporate heterocyclic moieties such as oxacyclohexanes. The model HA compound for this study merges the common functional groups found in HAs and combines them into a single, relatively small (<100 atoms) structure displayed in Figure 1.

Figure 1. Diagram of the humic acid model, HA, used to capture main functional groups known to be in humic substance in a relatively small number of atoms. HA^{-3} is a tri-anionic form of HA where carboxylic acid groups (arrows) are deprotonated.

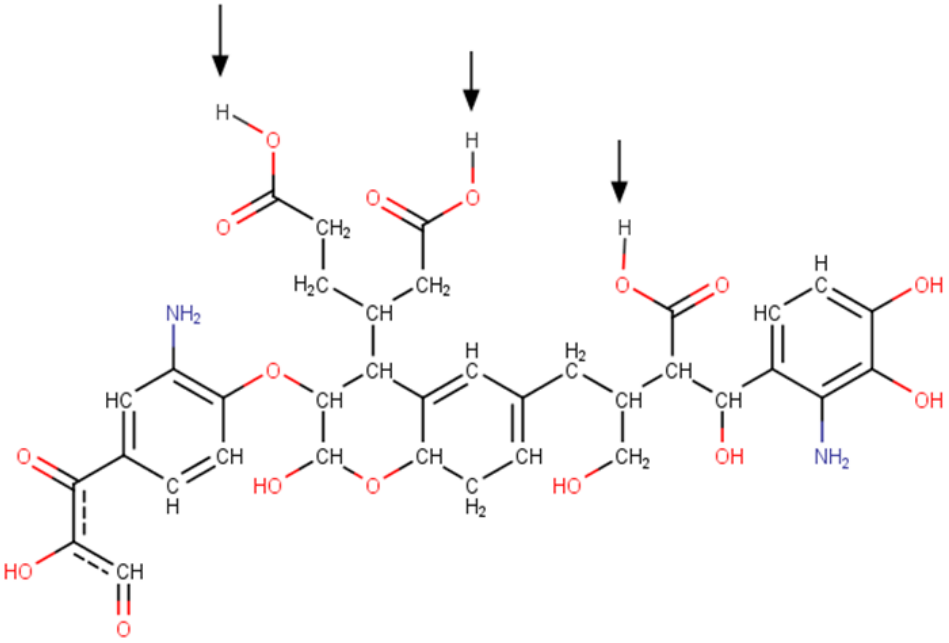

Figure 2. Defined structures for the munition compounds included in study. Acronym definitions for the munition compounds are as follows: DNAN -- 2,4-Dinitroanisole; NH4+DNi -- Ammonium Dinitramide; TNT – 2,4,6-Trinitrotoluene; NQ -- 1-Nitroguanidine; nMNA -- N-methyl-p-nitroaniline; RDX -- 1,3,5-Trinitro-1,3,5-triazinane; NTO -- 3-nitro-1,2,4-triazol-5-one (neutral form); NTO- -- conjugate base of NTO (anionic/deprotonated form).

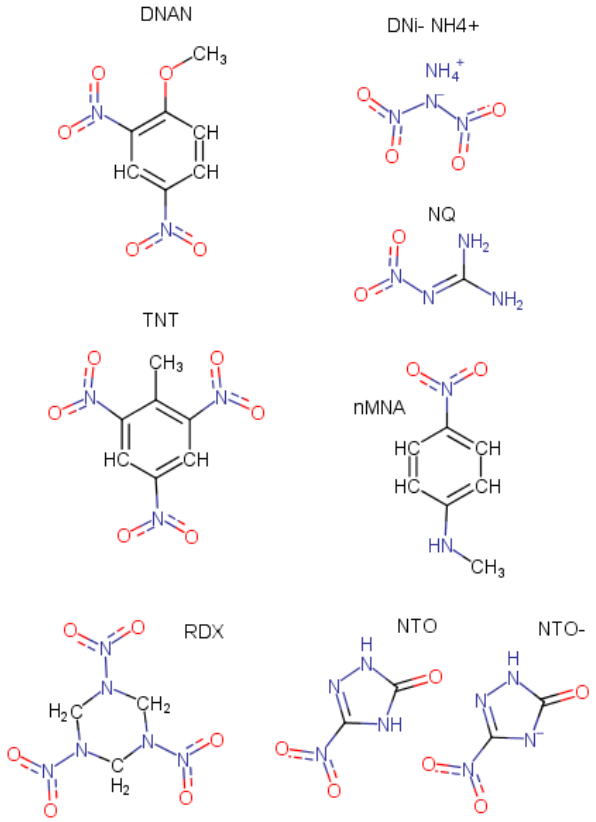

The munitions investigated in this study are depicted in Figure 2: 2,4-Dinitroanisole (DNAN), Ammonium Dinitramide ($[NH4]^+[DNi]^-$), N-methyl-p-nitroaniline (nMNA), 1-Nitroguanidine (NQ), 3-nitro-1,2,4-triazol-5-one (NTO) and its deprotonated form (NTO^{-1}), 1,3,5-Trinitro-1,3,5-triazinane (RDX) and 2,4,6-Trinitrotoluene (TNT). Each MC was modelled separately with the neutral HA model and the charged model, HA^{-3}, wherein the three carboxylic acids of the neutral version were deprotonated (Figure 1). The charge of each HA-IM pair was balanced by a number Na^+ or Cl^- ions added to the simulation box during the initial binding runs to achieve neutral net charge for the system. The $[DNi]^-$ ion was modelled separately from the $[NH4]^+[DNi]^-$ complex as the concentrations expected to occur in the environment are very low, and the ions will not remain tightly associated in water for a substantial length of time. Each MD System was created in packmol,[46] converted to an amber file by tleap, and the coordinates minimized for 2000 steps of steepest descent followed by 2000 steps of

conjugated gradient minimization in the Amber package.[30] The minimized simulation boxes were equilibrated in the isobaric isothermal ensemble (NPT) at 1 atm and 300 K for 1 ns or until the densities were constant. The equilibrated systems were simulated for an additional 5 ns at 1 atm and 300 K where solvent orientation, interactions, and conformations with the MC and ions were monitored. All MD simulations used a cut off for the short-range electrostatic interactions of 10 Å and the particle mesh Ewald algorithm for the long-range interactions.[47] The temperature was held constant at 300 K by a Langevin thermostat with a collision frequency of 20 ps^{-1}.[48] The time step for all simulations was 1 fs and the leapfrog algorithm was used for integrating the equations of motion.[49]

2.2 MD-docking/Structure generation

Docking of the MC and HA was achieved by 75 random trials and subsequent selection of the lowest energy configuration. At first the MC, HA, and counter ions for charge neutrality were simulated in a large, mostly empty box (40x40x40 Angstroms) at 300 K, where they would collide and stick at random relative locations. Then 2300 water molecules were added to the box and it was allowed to equilibrate density (i.e. NPT) and further refine the binding orientation and HA alignment for 0.5 ns for each system. Then the system was subjected to 20000 steps of steepest descent minimization followed by 20000 more steps of conjugated gradient minimization. The lowest-energy configuration of each HA-MC bound pair were saved. Coordinates for the minimized HA-MC pairs were then carried on to the TI studies and also extracted and optimized using DFT for the ionization potential (IP) and electron affinity (EA) calculations.

2.3 Thermodynamic Integration (TI)

Amber's pmemd version of TI was employed with softcore potentials and 9 lambda values following the appropriate Gaussian quadrature and associated weighting values. Isobaric, non-isochoric constraints were used to allow for decreasing system size when modeling the 'disappearance' of the MC from the bound state. The change in potential with respect to lambda was monitored and integrated to evaluate the solvation energy of the MC relative to the gas phase. Solvation energies of aqueous solubility were calculated and subtracted as well to reference the binding energy to HA relative to solvation by water. Each window within each replicate for each bound configuration was run for 10 ps. The TI calculations were repeated

10 times for each MC and the standard deviations in solvation energy were less than 10%.

2.4 Density Functional Theory (DFT)

The minimized structures from MD were optimized using the M06-2X functional and the 6-311G(d,p) basis set with CPCM implicit water solvation model as implemented in Gaussian 16 program and were used for the calculation of the redox properties.[36] The electron affinity (EA) and ionization potential (IP) of investigated systems were computed using the formula:

$$EA = E_{singlet} - E^{\bullet -} \quad (1)$$

$$IP = E^{\bullet +} - E_{singlet} \quad (2)$$

Where, $E_{singlet}$, $E^{\cdot -}$ and $E^{\cdot +}$ represent energy of the neutral, radical anionic and radical cationic species, respectively. For the computation of the vertical EA and IP values, the relevant radical anionic and cation energies corresponding to the ground state reference geometry were used. For the adiabatic EA and IP calculations the relevant radical anionic and cationic species were also separately optimized and their respective energies were used for the calculation. The redox potentials were calculated using equations 3-6[50]:

$$\Delta G_{red} = G^{\bullet -} - G_{singlet} \quad (3)$$

$$\Delta G_{ox} = G^{\bullet +} - G_{singlet} \quad (4)$$

$$E_{red} = E_H - \frac{\Delta G_{red}}{nF} \quad (5)$$

$$E_{ox} = E_H + \frac{\Delta G_{ox}}{nF} \quad (6)$$

where $G^{\bullet -}/G^{\bullet +}$represents the free energy of the radical anion/cation species, $G_{singlet}$ is the free energy of the singlet ground state species, E_{red}/E_{ox} are the redox potentials, n is the number of electrons transferred, F is the Faraday constant, and E_H is the standard hydrogen electrode potential (-4.28 eV).[51] The more positive reduction potential means more favorable radical anion state. In contrast, the more positive oxidation potential means less favorable radical cation state.

The DFT binding energies were calculated by subtracting the energies of the sum of the monomers within the complex geometry from the energy of the complex. Since, basis set superposition error (BSSE) computation is not available in the implicit solvation model, therefore, such error was computed in the gas phase using the complex geometries optimized in the CPCM implicit solvation model and the counterpoise correction scheme as implemented in Gaussian16. The binding energies calculated within the CPCM implicit solvation were then corrected by the gas-phase BSSE. The BSSE correction is not expected to change with respect to implicit solvation and has been applied in this way previously.[52]

3 Results and Discussion

3.1 Hydrogen bonding

The presence of a hydrogen bond from the MD trajectories was characterized by a distance under 3 Å between the acceptor and donor heavy atom, and an angle of 135° to 225° between a heavy atom, a hydrogen, and the other heavy atom. These distance and angle cutoffs are in accordance with the defaults for cpptraj,[53] and are relatively stringent to ensure comparison of only the most definitive hydrogen bonds. Data was included from all of the configurations and binding locations (not limited to the lowest energy bound states) to increase sampling accuracy of the hydrogen bond dynamics. The averaged results, shown in Table 1, indicate that most of the MC-water interactions are unchanged by the protonation state of the HA. Conversely, the HA-water interactions are increased by deprotonation of the carboxylic acids by forming an average of an additional 5 hydrogen bonds with water molecules. This indicates the HA will interact more with the water when the carboxyl groups are deprotonated (HA^{-3} form) as compared to the neutral form (HA). Hydrogen bonding also occurs intra-molecularly between different sites within the same HA model as it folds and bends. The intramolecular hydrogen bonding within the HA^{-3} is increased by 1 hydrogen bond on average relative to the neutral structure. This occurs because the ratio of proton donating and accepting sites on the HA are closer to balanced when the carboxyl groups are not protonated. These changes in H-bonding help to explain why the solvation energy for the HA^{-3} is so much larger than for HA.

On the other hand, the hydrogen bonding interactions between the HA and MC are generally species dependent and sensitive to the protonation state of HA. For example, the hydrogen bonding averages for NTO were higher with HA^{-3} as compared to HA, and the reverse is true for NTO^-. These flipped H-bonding opportunities make sense intuitively and also align with the thermodynamic integration (TI) energy calculations. These results suggest that certain pH range can be used to control the binding of NTO with HA. For example, acidic conditions specifically in the pH range between the pKa values of NTO (3.76) and HA (1.7-2.5) will lead to stronger binding between the neutral NTO and the anionic HA as compared to at pHs either below 1.7 or above 3.8 where NTO and HA are both protonated or both unprotonated respectively. Furthermore, our simulated results help explain the experimental column transport findings of

Mark *et. al.*[27,28] which show a strong inverse relationship between the pH of the soil in the column and the absorption coefficient of the NTO.

Table 1. Average number of hydrogen bonds in between species-pairs at any particular snapshot in the MC-HA bound complexes in water solution. The species pairs are represented in the form of MC/Water, HA/Water, HA/MC and HA/HA pairs where HA/HA pair is due to the formation of intramolecular hydrogen bonds.

	MC/Water		HA/Water		HA/MC		HA/HA	
MC	HA	HA^{-3}	HA	HA^{-3}	HA	HA^{-3}	HA	HA^{-3}
DNAN	1.7	1.8	22.2	27.4	0.02	0.02	0.5	1.3
DNi^{-}	2.6	2.7	21.9	26.4	0.01	0.01	0.5	1.3
NH_4^+	2.1	2.0	22.1	28.1	0.07	0.26	0.5	1.3
nMNA	1.7	1.7	22.1	27.3	0.03	0.02	0.5	1.4
NQ	2.1	2.1	22.2	27.3	0.02	0.06	0.5	1.2
NTO	2.9	2.9	22.2	27.1	0.04	0.11	0.4	1.2
NTO^{-}	5.5	5.3	21.7	27.1	0.16	0.07	0.5	1.1
RDX	2.1	2.1	22.1	27.2	0.02	0.04	0.5	1.2
TNT	2.1	2.2	22.2	27.4	0.03	0.02	0.5	1.2

MC=munition compound, Water=solvent interactions, HA=humic acid.

3.2 Binding between munition and humic substances

TI calculations of the solvation free energy include explicit solvent molecules, capture changes in the solvent-solvent interactions caused by the solute, and the solute-solvent interactions. Consequently, they have increased variability and are also more directly comparable to experiment as compared to the interaction potentials from DFT without explicit solvation. As a validation to ensure the method is producing reasonable results, we calculated the solvation free energy of water in water to be 9.2 +/-0.5 kcal/mol, which for this relatively high-throughput method and TIP3P parameters is a reasonable approximation of the real value of 8.5 kcal/mol determined by Hummer *et al.*[54] through more rigorous methods, including fluctuation statistical analysis and Bennett's Methods[55]. Although, this study is utilizing less rigorous methods than Hummer *et al.*[54] the methods are suitable for qualitative observations and analysis of the trends. Table 2 summarizes the TI results for each species with the HA and anionic HA and the difference with respect to pure water solvation. Ionic species have relatively large free energies of solvation (ΔG) due to contributions not just from direct munition-water interactions but also the induced water ordering in extended solvation shells around the ion. Not surprisingly, MCs with aromatic rings - DNAN, nMNA, and TNT - exhibit some of the strongest free energy of binding ($\Delta\Delta G$), as non-polar moieties are generally the least

favorably-solvated in water and π stacking with the HA strongly influences solvation.[56] For reference a Boltzmann distribution of two states based on -3.3 kcal/mol (TNT with HA) difference in free energy translates to a 10^2-fold difference in population of states. This order of magnitude is on par with some of the K_d values for TNT in high humic-containing soils, the highest being around K_d = 100 L/kg[4] and likewise for RDX with -2.6 kcal/mol yielding a Boltzmann weight of about order 10^1-10^2 and highest reported K_d in soil around K_d = 20 L/kg.[4]

Table 2. Average Gibbs free binding energies of munition to HA from thermodynamic integration (TI) in kcal/mol. Standard deviations are about 1.7 kcal/mol for each system.

IM	$\Delta G_{solvation}$ in Water	$\Delta G_{solvation}$ bound with HA	$\Delta G_{solvation}$ bound with HA^{-3}	ΔG_{HA} - ΔG-Water	$\Delta G_{HA^{-3}}$ - ΔG-Water
DNAN	-19.1	-22.1	-18.9	-3.0	0.1
DNi^- **	-77.4	-77.8	-77.5	-0.4	-0.1
NH_4^+ **	-67.9	-68.0	-67.8	-0.1	0.1
nMNA	-12.8	-15.2	-15.1	-2.4	-2.3
NQ **	-13.3	-13.7	-13.8	-0.5	-0.6
NTO	-17.0	-17.8	-17.8	-0.9	-0.8
NTO^-	-83.3	-86.4	-87.2	-3.1	-3.9
RDX	-22.6	-25.2	-21.8	-2.6	0.9
TNT	-20.2	-23.5	-21.5	-3.3	-1.3
HA*	-148	NA	NA	NA	NA
HA^{-3}*	-419	NA	NA	NA	NA

*The values listed for humic acid are solvation free energies for each HA without any munition (+-10 kcal/mol for HA).

**These compounds would not stay bound without restraints – ΔΔG values are close to zero due to being mostly solvated by water and subtracting the water solvation free energy.

Interestingly the NTO^- anion exhibits a binding energy on par with the aromatic compounds. This finding is corroborated by experimental soil column studies which found the retention of NTO to positively correlate with the fraction of organic carbon content in the soil.[27,28] Examination of the binding modes reveals that the most favorable binding for NTO^- with either form of HA is through interactions of the deprotonated nitrogen site with the alkyl regions of the HA. As seen by correlating the differences between NTO and NTO^- this conformational shift causes increased H-bonding between MC and HA as well as optimizing H-bonding between the MC and water.

The BSSE corrected binding energy of the most stable MC-HA/HA^{3-} complexes at the M06-2X/6-311G(d,p) level in the implicit water environment shows that MCs bind favorably to both the neutral and ionic form of HA (Table 3). The protonation state of the two molecules has a large impact on the binding energy which can be important at certain pH ranges. For example, NTO binds strongly to the conjugate base HA^{-3}; however, it only binds weakly to the neutral HA, which is in agreement with the results from the TI. The case where NTO is protonated (neutral) and the HA is anionic is only expected to occur between the pKa's of the two structures, as previously mentioned that corresponds to pHs around 2 to 3.5. Below a pH of 2 all the species will likely be protonated and NTO binding will be weak, at pH's between 2 and 3.5 the HA might be deprotonated and the neutral NTO will bind to HA^{-3} strongly, however at pHs above 3.5, when NTO^- is also anionic the binding with HA^{-3} will again be weak. A similar trend is observed for DNi^- binding to HA with binding in strong acidic conditions being weak and going to outright unfavorable in most of the pH range where HA^{-3} is deprotonated.

Table 3. The BSSE-corrected binding energies (kcal/mol) for the lowest energy configuration of munition compounds with humic acid (neutral and tri-anionic forms) complexes calculated at CPCM/M06-2X/6-311G(d,p) level.

Munition	HA	HA^{-3}
DNAN	-18	-12
DNi^-	-8	6
nMNA	-16	-16
NQ	-18	-12
NTO	-4	-23
NTO^-	-6	-8
RDX	-15	-16
TNT	-13	-14

3.3 Ionization Potentials (IP) and Electron Affinities (EA)

For a basis of comparison, the IP, EA and redox properties were calculated for each compound individually and are depicted in the Figure 3 and also tabulated in Table S2 of the supporting information. The computed IP, EA, and redox values of MCs are in close agreement with previous literature.[50] These values for HA and HA^{-3} were also computed at the CAM-B3LYP/6-311G(d,p) and M06-2X/6-311G(d,p) levels in the bulk water using SMD and CPCM solvation model to ensure reproducibility across different DFT functionals and solvation models. In all cases the results were within 0.4

eV from each other with negligible spin contamination and are reported in the Supporting Information Table S3.

It is intriguing that the protonation state of the HA does not seem to have much impact on the ionization and oxidation potentials implying that it takes nearly equivalent energy to remove an additional electron from the neutral and anionic forms of the HA. Note that both HA species have a significantly lower ionization and oxidative potentials than most of the MCs indicating that in isolation under oxidative conditions the HA will forfeit an electron more readily than the MC. On the other hand, the EA of anionic HA^{-3}, as would be most common protonation state under environmental pH, is lower than the EA of any of the MCs. This indicates that under the normal environmental condition isolated HA will be more difficult to reduce than isolated MCs.

Looking at the MCs individually we notice that MCs with substantial aromaticity such as DNAN, TNT, nMNA, and NTO exhibit relatively higher EA and reductive potential than the non-aromatic MCs (Figure 3). This results from the combination of conjugation and nitro groups withdrawing electron density from the aromatic ring. This distributed electron-withdrawn region serves to host and stabilize the extra electron in radical anion state of aromatic MCs with a lower energy penalty compared to non-aromatic MCs. Beyond the isolated compounds, once complexation with the HA^{-3} occurs, stacking of the aromatic regions can synergistically stabilize the radical anion state.[57] This explains the relatively higher EA values for complexes between HA^{-3} and aromatic MCs as shown in the Table 4.

Figure 3. The redox (bottom rectangle) and EA/IP (top rectangle) properties of isolated MC and HA compounds.

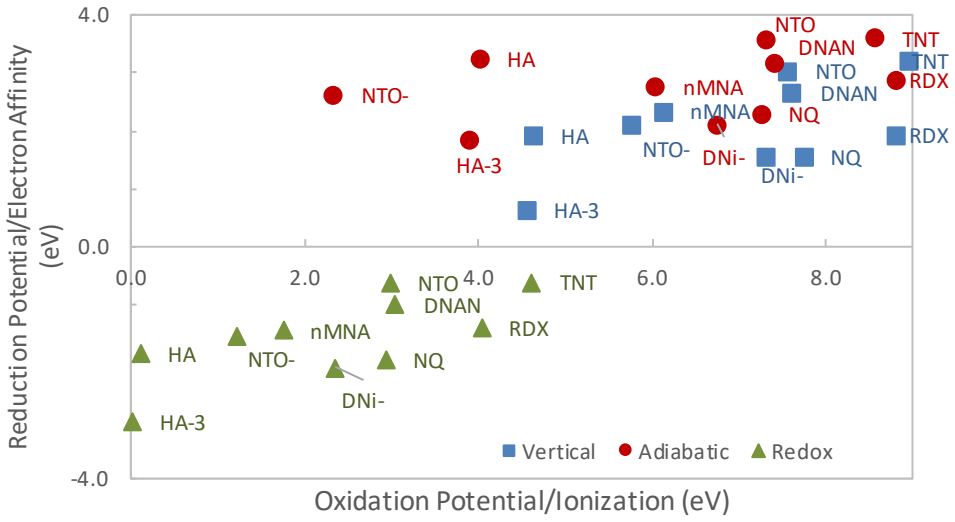

Table 4. Ionization potential (IP), electron affinity (EA), oxidation and reduction potentials for each of the complexed munition-humic systems with CPCM implicit solvent at M06-2X/6-311G(d,p) level. All energies are in eV.

Bound System		Vertical ionization		Adiabatic ionization		Redox	
Munition	Humic	IP-vert	EA-vert	IP-adia	EA-adia	Oxidation	Reduction
DNAN	HA	4.2	3.5	4.0	3.9	-0.3	-0.4
DNi^-	HA	4.4	1.7	4.1	2.5	-0.2	-1.7
nMNA	HA	4.3	3.5	4.0	3.8	-0.3	-0.4
NQ	HA	4.3	3.6	4.0	4.1	-0.3	0.0
NTO	HA	4.2	3.6	4.0	3.9	-0.4	-0.3
NTO^-	HA	4.4	1.8	4.1	2.2	-0.1	-2.1
RDX	HA	4.5	3.6	4.2	4.1	-0.1	-0.1
TNT	HA	4.6	3.0	4.2	3.3	-0.2	-0.8
DNAN	HA^{-3}	4.3	2.5	3.9	2.9	-0.4	-1.2
DNi^-	HA^{-3}	4.2	1.8	3.9	2.5	-0.4	-1.8
nMNA	HA^{-3}	4.2	3.3	3.9	3.6	-0.4	-0.7
NQ	HA^{-3}	4.2	1.0	3.9	1.9	-0.5	-2.4
NTO	HA^{-3}	4.2	2.5	3.9	3.6	-0.4	-0.4
NTO^-	HA^{-3}	4.2	1.7	3.9	2.1	-0.4	-2.2
RDX	HA^{-3}	4.2	2.1	3.9	2.7	-0.4	-1.4
TNT	HA^{-3}	4.4	3.1	4.0	3.4	-0.3	-0.8

The lowest energy bound structure for each HA-MC pair from MD simulation were reoptimized at the M06-2X/6-311G(d,p) level in the bulk water

using the CPCM approach, and their computed IP, EA, and redox properties are listed in Table 4. The EA of HA^{-3} tends to increase under complexation with MCs and the EA and reductive potential values are generally lower in the MC-HA^{-3} complex than the corresponding MC-HA complex. These trends indicate that complexation between MC and HA^{-3} tends to increase the ability for the HA^{-3} to be reduced, but not to the point of surpassing the neutral form of HA which will undergo reduction easier than individual HA^{-3} or MC-HA^{-3} complexes.

Ionization and oxidation potentials of all HA-MC complexes are generally very similar regardless of the MC that is bound in the system (Table 4). Moreover, these values are very similar to those computed for HA and its anionic form. The analysis of highest occupied molecular orbital (HOMO) and lowest unoccupied molecular orbital (LUMO) of these complexes show that HOMO is consistently located in the same spot on the HA; distributed across the aldehyde end of the molecule (left side of Figures 1 and 4). This region of the HA model has a relatively high degree of conjugation and electron donating groups making it the preferred spot to undergo oxidation. Thus, our results show that in the studied complexes the HA part will undergo electronic ionization. On the other hand, the location of the LUMO in all complexes varies dramatically. This suggests that the preferred location for reductive attack will depend on adsorbed species and HA conformation. Notably, the presence of MCs influences the preferred conformation of the HA and hence the reduction potential and EA changes even when the MC is not directly involved in the radical formation. Moreover, HA is large system and it is expected that it will have several conformations with similar energy.

While oxidation tends to occur on the HA rather than the MC, reduction, on the other hand, is located on the HA in roughly half of the systems and at least partially on the MC in the other half of the systems. Figure 4 depicts an example of these orbitals for TNT bound to HA^{-3}. The LUMO, indicative of the reduction site, for the complex, is centered on the TNT while the HOMO, indicative of the oxidation site, is located on the aldehyde end of the HA^{-3}. For comparison, the HOMO and LUMO for each individual species are shown in SI (Figures S1-S11). Despite HAs individually exhibiting a lower reductive potential than the individual MCs the orbital locations of the bound systems indicate that while bound to MCs the HAs ionize instead of the MC about half of the time.

Figure 4. HOMO and LUMO orbital densities for TNT-HA^{-3} complex. The HOMO is localized on the aldehyde end of HA (left side) and the LUMO is localized on TNT (top left).

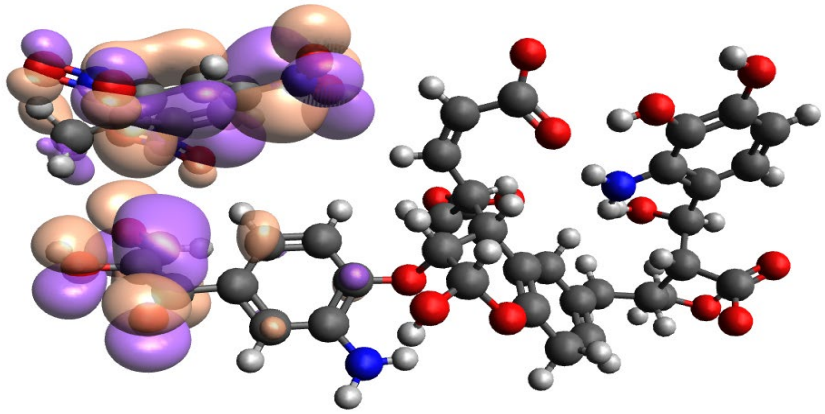

Table 5. Ionization potential (IP), electron affinity (EA), oxidation and reduction potentials for each of the conformations of HA individually with CPCM implicit solvent at M06-2X/6-311G(d,p) level. All energies are in eV.

Humic System	Vertical ionization		Adiabatic ionization		Redox	
(Conformation)	IP-vert	EA-vert	IP-adia	EA-adia	Oxidation	Reduction
$HA_{(HA\text{-}DNAN)}$	4.2	3.6	4	3.8	0	-0.7
$HA_{(HA\text{-}DNi\text{-})}$	4.4	1.5	4.1	1.9	0.2	-2.7
$HA_{(HA\text{-}nMNA)}$	4.3	3.6	4	3.9	0.1	-0.7
$HA_{(HA\text{-}NQ)}$	4.3	3.7	4	4.1	0.1	-0.7
$HA_{(HA\text{-}NTO)}$	4.2	3.5	4	3.9	0	-0.6
$HA_{(HA\text{-}NTO\text{-})}$	4.4	1.5	4.1	1.9	0.2	-2.7
$HA_{(HA\text{-}RDX)}$	4.3	3.7	4	4	0.1	-0.7
$HA_{(HA\text{-}TNT)}$	4.4	1.7	4.1	2.5	0.2	-2.6
Average HA	4.3(0.1)	2.8(1.1)	4.0(0.1)	3.3(1.0)	0.1 (0.1)	-1.4 (1.0)
$HA^{-3}{}_{(HA3\text{-}DNAN)}$	4.2	0.4	3.9	0.8	0	-3.8
$HA^{-3}{}_{(HA3\text{-}DNi\text{-})}$	4.2	0.6	3.9	3.4	0	-3.5
$HA^{-3}{}_{(HA3\text{-}nMNA)}$	4.2	3.3	3.9	3.6	0	-1
$HA^{-3}{}_{(HA3\text{-}NQ)}$	4.2	0.4	3.9	1	0	-3.9
$HA^{-3}{}_{(HA3\text{-}NTO)}$	4.2	0.5	3.9	0.9	0	-3.9
$HA^{-3}{}_{(HA3\text{-}NTO\text{-})}$	4.2	0.4	3.9	0.8	0	-3.9
$HA^{-3}{}_{(HA3\text{-}RDX)}$	4.2	0.4	3.9	0.8	0	-3.9
$HA^{-3}{}_{(HA3\text{-}TNT)}$	4.2	3.1	4	3.4	0	-1.2
Average HA^{-3}	4.2(0.0)	1.1(1.3)	3.9(0.0)	1.8(1.3)	0.0 (0.0)	-3.1 (1.3)

The changes in ionization potential and electron affinity of HA may be impacted not only by presence of the MC but also by the conformational changes induced by the MC binding. Table 5 lists the IP, EA, and redox

properties associated with HA in each of the MC-HA complex conformations. In these calculations, the HA part in each of the complex was separately optimized at the M06-2X/6-311G(d,p) level in the water solution using CPCM approach. The optimized geometry of HA was found to retain its configuration in the corresponding MC-HA complex within an RMSD of 1 Å. Computed results show that the IP and oxidation values are largely independent of conformation or protonation state of the HA. Alternatively, the EA and reduction potentials are highly contingent upon protonation state of HA (Table 5). This result can be explained by the increased electron donating character of carboxylate ions relative to carboxylic acid in water.

Comparing the results in Table 5 against the results with the HA-MC bound complexes included in Table 4, we note that both changes to the HA conformation and electronic influences of binding with MCs can lower the barriers to HA ionization. Table S1 in the supporting information explicitly shows the differences in IP/EA/redox between the HAs of each conformation with and without MC. Changes to the IP are mild, with a minor increase on average, and changes to the EA are relatively large, 0.6 eV increase on average. The oxidative potential decreases in the absence of MCs by an average of -0.4 eV and the reductive potential increases by an average of 1.2 eV. These changes indicate that the presence of MCs with the HA significantly increase the chance of HA being radicalized instead of the MC when the two are bound together. This trend has implications for environmental persistence of released MCs and may inform fate and transport modeling as well as soil type selection for range management at explosive training grounds.

Degradation of the MCs typically involves oxidizing or reducing agents; however, based on these results the HA will respond more readily to both oxidizing and reducing agents as compared to the MCs. The HA buffers the MC against the gain and loss of electrons and hence also buffers against the degradation of bound MC compounds. These results align with and help explain the results of Martin *et. al.* [29] on the role of humic acid in fate and transport of compounds in the environment. Although HA may bind and contain the MCs to a local area in remediation situations, it is predicted to adversely impact the potential to degrade MCs due to buffering against oxidative and reductive agents.

4 Conclusions

Calculations of the binding energies, ionization potentials, and electron affinities elucidate binding and potential degradation motifs of MCs with HAs including the impact of explicit intermolecular interactions with solvent and MC. HAs readily bind to most MCs and binding strength correlates with optimizing hydrogen bonding between solvent, HAs, and MCs. The pH dependence on binding, particularly in respect to NTO, predicts that the tightest binding of NTO to HA will occur in solutions of around pH 2 to pH 3. HAs can act both as a source and sink for electrons and radicalize more readily than the MCs under oxidative conditions. When HA and MC are complexed, both oxidation and reduction can radicalize the HA instead of the MC. Thus, the presence of HA can increase the stability of MCs and have an adverse impact on remediation efforts by buffering against both oxidizing and reducing agents that otherwise would catalyze degradation of MCs in the environment.

Abbreviations

DNAN -- 2,4-Dinitroanisole

HA -- Neutral form of the humic acid model

HA^{-3} -- Deprotonated form of the humic acid model

MC – Munition Compounds and legacy high explosives

$[NH4]^{+}[DNi]^{-}$ -- Ammonium Dinitramide

nMNA -- N-methyl-p-nitroaniline

NQ -- 1-Nitroguanidine

NTO -- 3-nitro-1,2,4-triazol-5-one (Neutral form)

NTO^{-} -- 3-nitro-1,2,4-triazol-5-one (Deprotonated form)

RDX -- 1,3,5-Trinitro-1,3,5-triazinane

TNT – 2,4,6-Trinitrotoluene

Supporting information description

The supporting information document includes additional figures mapping the orbital locations, table of differences in the bound and unbound electronic properties of the systems, and table of validation data for the independence on DFT functional. The Supporting Information is available free of charge at https://pubs.acs.org/doi/10.1021/acs.jpca.0c08177.

References

(1) Vereecken, H.; Schnepf, A.; Hopmans, J. W.; Javaux, M.; Or, D.; Roose, T.; Vanderborght, J.; Young, M. H.; Amelung, W.; Aitkenhead, M.; et al. Modeling Soil Processes: Review, Key Challenges, and New Perspectives. *Vadose Zo. J.* **2016**, *15*, 0.

(2) Peña-méndez, M. E.; Havel, J.; Patočka, J. Humic Substances – Compounds of Still Unknown Structure : Applications in Agriculture , Industry , Environment , and Biomedicine. *J. Appl. Biomed.* **2005**, *3*, 13–24.

(3) Thorn, K. A.; Kennedy, K. R. N-15 NMR Investination of the Covalent Binding of Reduced TNT Amines to Soil Humic Acid, Model Compounds, and Lignocellulose. *Environ. Sci. Technol.* **2002**, *36*, 3787–3796.

(4) Lotufo, G. R.; Chappell, M. A.; Price, C. L.; Ballentine, M. L.; Fuentes, A. A.; Bridges, T. D.; George, R. D.; Glisch, E. Review and Synthesis of Evidence Regarding Environmental Risks Posed by Munitions Constituents (MC) in Aquatic Systems. **2017**, *ERDC/EL TR*, 254.

(5) Eriksson, J.; Skyllberg, U. Binding of 2,4,6-Trinitrotoluene in a Soil Organic Matter Two-Phase System. *J. Envir* **2001**, *30*, 2053–2061.

(6) Atherton, N. M.; Cranwell, P. A.; Floyd, A. J.; Haworth, R. D. Humic Acid I: ESR Spectra of Humic Acids. *Tetrahedron* **1967**, *23*, 1653–1667.

(7) Abbt-Braun, G.; Lankes, U.; Frimmel, F. H. Structural Characterization of Aquatic Humic Substances - The Need for a Multiple Method Approach. *Aquat. Sci.* **2004**, *66*, 151–170.

(8) Cheshire, M. V.; Cranwell, P. A.; Falshaw, C. P.; Floyd, A. J.; Haworth, R. D. Humic Acid-II. Structure of Humic Acids. *Tetrahedron* **1967**, *23*, 1669–1682.

(9) Greene, G.; Steelink, C. Structure of Soil Humic Acid. II. Copper Oxidation Products. *J. Org. Chem.* **1962**, *27*, 170–174.

(10) Leenheer, J. A.; Croue, J.-P. Characterizing Aquatic Dissolved Organic Matter. *Environ. Sci. Technol.* **2003**, *37*, 18–26.

(11) Gauthier, T. D.; Seitz, W. R.; Grant, C. L. Effects of Structural and Compositional Variations of Dissolved Humic Materials on Pyrene Koc Values. *Environ. Sci. Technol.* **1987**, *21*, 243–248.

(12) Westall, J. C.; Jones, J. D.; Turner, G. D.; Zachara, J. M. Models for Association of Metal Ions with Heterogeneous Environmental Sorbents. 1. Complexation of Co(II) by Leonardite Humic Acid as a Function of PH and NaClO4Concentration. *Environ. Sci. Technol.* **1995**, *29*, 951–959.

(13) Sutton, R.; Sposito, G. Molecular Structure in Soil Humic Substances: The New View. *Environ. Sci. Technol.* **2005**, *39*, 9009–9015.

(14) Zepp, R. G.; Braun, A. M.; Holane, J.; Leenheer, J. A. Photoproduction of Hydrated Electrons from Natural Organic Solutes in Aquatic Environments. *Environ. Sci. Technol.* **1987**, *21*, 485–490.

(15) Chorover, J.; Amistadi, M. K.; Burgos, W. D.; Hatcher, P. G. Quinoline

Sorption on Kaolinite-Humic Acid Complexes. *Soil Sci. Soc. Am. J.* **1999**, *63*, 850–857.

(16) Perminova, I. V.; Grechishcheva, N. Y.; Petrosyan, V. S. Relationships between Structure and Binding Affinity of Humic Substances for Polycyclic Aromatic Hydrocarbons: Relevance of Molecular Descriptors. *Environ. Sci. Technol.* **1999**, *33*, 3781–3787.

(17) Alvarez-Puebla, R. A.; Valenzuela-Calahorro, C.; Garrido, J. J. Theoretical Study on Fulvic Acid Structure, Conformation and Aggregation: A Molecular Modelling Approach. *Sci. Total Environ.* **2006**, *358*, 243–254.

(18) Walsh, M. R.; Walsh, M. E.; Ramsey, C. A.; Thiboutot, S.; Ampleman, G.; Diaz, E.; Zufelt, J. E. Energetic Residues from the Detonation of IMX-104 Insensitive Munitions. *Propellants, Explos. Pyrotech.* **2014**, *39*, 243–250.

(19) Reddy, G.; Song, J.; Kirby, P.; Lent, E. M.; Crouse, L. C. B.; Johnson, M. S. Genotoxicity Assessment of an Energetic Propellant Compound, 3-Nitro-1,2,4-Triazol-5-One (NTO). *Mutat. Res. - Genet. Toxicol. Environ. Mutagen.* **2011**, *719*, 35–40.

(20) Kennedy, A. J.; Lounds, C. D.; Melby, N. L.; Laird, J. G.; Winstead, B.; Brasfield, S. M.; Johnson, M. S. *ERDC-Technical Report: Development of Environmental Health Criteria for Insensitive Munitions : Aquatic Ecotoxicological Exposures Using*; **2013**.

(21) Olivares, C. I.; Sierra-Alvarez, R.; Abrell, L.; Chorover, J.; Simonich, M.; Tanguay, R. L.; Field, J. A. Zebrafish Embryo Toxicity of Anaerobic Biotransformation Products from the Insensitive Munitions Compound 2,4-Dinitroanisole. *Environ. Toxicol. Chem.* **2016**, *35*, 2774–2781.

(22) Linker, B. R.; Khatiwada, R.; Pedrial, N.; Abrell, L.; Sierra, R.; Field, J. A.; Chorover, J. Adsorption of Novel Insensitive Munitions Comounds at Clay Mineral and Metal Oxide Surfaces. *Environ. Chem.* **2015**, *12*, 74–84.

(23) Hawari, J.; Monteil-rivera, F.; Perreault, N. N.; Halasz, A.; Paquet, L.; Radovic-hrapovic, Z. Chemosphere Environmental Fate of 2 , 4-Dinitroanisole (DNAN) and Its Reduced Products. *Chemosphere* **2015**, *119*, 16–23.

(24) Allen, H.; Toro, D. Di; Ta, D.; Kuo, F.; Michelson, K.; Miglino, A.; Checkai, R.; Kuperman, R.; Simini, M.; Edgewood, U. S. A.; et al. SERDP Technical Report ER-1688 - Improving Understanding of the Fate and Transport of Munitions Constituents to Enhance Sustainability of Operational Ranges. **2015**.

(25) Uchimiya, M.; Gorb, L.; Isayev, O.; Qasim, M. M.; Leszczynski, J. One-Electron Standard Reduction Potentials of Nitroaromatic and Cyclic Nitramine Explosives. *Environ. Pollut.* **2010**, *158*, 3048–3053.

(26) Xia, K.; Bleam, W.; Helmke, P. A. Studies of the Nature of Binding Sites of First Row Transition Elements Bound to Aquatic and Soil Humic Substances Using X-Ray Absorption Spectroscopy. *Geochim. Cosmochim. Acta* **1997**, *61*, 2223–2235.

(27) Mark, A. J.; Dontsova, K. M.; Brusseau, M.; Taylor, S. Adsorption and

Attenuation Behavior of 3-Nitro-1,2,4-Triazole-5-One (NTO) in Eleven Soils. *Chemosphere* **2016**, *144*, 1249–1255.

(28) Mark, A. J.; Dontsova, K. M.; Brusseau, M.; Taylor, S.; Jiri Simunek, J. Column Transport Studies of 3-Nitro-1,2,4-Triazole-5-One (NTO) in Soils. *Chemosphere* **2017**, *171*, 427–434.

(29) Martin, D. P.; Seiter, J. M.; Lafferty, B. J.; Bednar, A. J. Exploring the Ability of Cations to Facilitate Binding between Inorganic Oxyanions and Humic Acid. *Chemosphere* **2017**, *166*, 192–196.

(30) D.A. Case, J. T. B., R.M. Betz, D.S. Cerutti, T.E. Cheatham III, T.A. Darden, R. E. D., T.J. Giese, H. Gohlke, A.W. Goetz, et al. Amber Molecular Dynamics. University of California: San Francisco 2016.

(31) Sprenger, K. G.; Jaeger, V. W.; Pfaendtner, J. The General AMBER Force Field (GAFF) Can Accurately Predict Thermodynamic and Transport Properties of Many Ionic Liquids. *J. Phys. Chem. B* **2015**, *119*, 5882–5895.

(32) Wang, J., Wolf, R. M.; Caldwell, J. W.;Kollman, P. A.; Case, D. A. Development and Testing of a General AMBER Force Field. *J. Comput. Chem.* **2004**, *25*, 1157–1174.

(33) Wang, J., Wang, W., Kollman P. A.; Case, D. A. Automatic Atom Type and Bond Type Perception in Molecular Mechanical Calculations. *J. Mol. Graph. Model.* **2006**, *25*, 247260.

(34) Møller, C.; Plesset, M. S. Note on an Approximation Treatment for Many-Electron Systems. *Phys. Rev.* **1934**, *46*, 618–622.

(35) Dunning Jr., T. H. Gaussian Basis Sets for Use in Correlated Molecular Calculations. 1. The Atoms Boron through Neon and Hydrogen. *J. Chem. Phys.* **1989**, *90*, 1007–1023.

(36) Frisch, M. J. .; Trucks, G. W. .; Schlegel, H. B. .; Scuseria, G. E. .; Robb, M. A. .; Cheeseman, J. R. .; Scalmani, G.; Barone, V. .; Petersson, G. A. .; Nakatsuji, H.; et al. Gaussian16, Revision B.01. Gaussian Inc., Wallingford CT 2016.

(37) Zhang, Y.; Maginn, E. J. A Simple AIMD Approach to Derive Atomic Charges for Condensed Phase Simulation of Ionic Liquids. *J. Phys. Chem. B* **2012**, *116*, 10036–10048.

(38) Sambasivarao, S. V.; Acevedo, O. Development of OPLS-AA Force Field Parameters for 68 Unique Ionic Liquids. *J. Chem. Theory Comput.* **2009**, *5*, 1038–1050.

(39) Schutt, T. C.; Bharadwaj, V. S.; Hegde, G. A.; Johns, A. J.; Maupin, C. M. In Silico Insights into the Solvation Characteristics of the Ionic Liquid 1-Methyltriethoxy-3-Ethylimdazolium Acetate for Cellulosic Biomass. *Phys. Chem. Chem. Phys.* **2016**, *18*, 23715–23726.

(40) Bharadwaj, V. S.; Schutt, T. C.; Ashurst, T. C.; Maupin, C. M. Elucidating the Conformational Energetics of Glucose and Cellobiose in Ionic Liquids. *Phys. Chem. Chem. Phys.* **2015**, *17*, 10668–10678.

(41) Jorgensen, W.; Chandrasekhar, J.; Madura, J.; Klein, M. Comparison of Simple Potential Functions for Simulating Liquid Water. *J. Chem. Phys.*

1983, *79*, 926–935.
(42) Sviatenko, L. K.; Gorb, L.; Shukla, M. K.; Seiter, J. M.; Leszczynska, D.; Leszczynski, J. Adsorption of 2,4,6,8,10,12-Hexanitro-2,4,6,8,10,12-Hexaazaisowurtzitane (CL-20) on a Soil Organic Matter. A DFT M05 Computational Study. *Chemosphere* **2016**, *148*, 294–299.
(43) Sein, L. T.; Varnum, J. M.; Jansen, S. A. Conformational Modeling of a New Building Block of Humic Acid: Approaches to the Lowest Energy Conformer. *Environ. Sci. Technol.* **1999**, *33*, 546–552.
(44) Lan, T.; Liao, J.; Yang, Y.; Chai, Z.; Liu, N.; Wang, D. Competition/Cooperation between Humic Acid and Graphene Oxide in Uranyl Adsorption Implicated by Molecular Dynamics Simulations. *Environ. Sci. Technol.* **2019**, *53*, 5102–5110.
(45) Petrov, D.; Tunega, D.; Gerzabek, M. H.; Oostenbrink, C. Molecular Dynamics Simulations of the Standard Leonardite Humic Acid: Microscopic Analysis of the Structure and Dynamics. *Environ. Sci. Technol.* **2017**, *51*, 5414–5424.
(46) Martinez, L.; Andrade, R.; Birgin, E. G.; Martinez, J. M. PACKMOL: A Package for Building Initial Configurations for Molecular Dynamics Simulations. *J. Comput. Chem.* **2009**, *30*, 2157–2164.
(47) Darden, T.; York, D.; Pedersen, L. Particle Mesh Ewald–an Nlog(N) Method for Ewald Sums in Large Systems. *J. Chem. Phys.* **1993**, *98*, 10089–10092.
(48) Pastor, R.; Brooks, B.; Szabo, A. An Analysis of the Accuracy of Langevin and Molecular Dynamics Algorithms. *J. Mol. Phys.* **1988**, *65*, 1409–1419.
(49) Van Gunsteren, W. F.; Berendsen, H. J. C. A LEAP-FROG ALGORITHM FOR STOCHASTIC DYNAMICS. *Mol. Simul.* **1988**, *1*, 173–185.
(50) McAlexander, H. R.; Giles, S.; Crouch, R. A.; Peel, H. An Integrated Quantum Chemical and Experimental Approach for Exploring the Structures and Properties of Insensitive Munitions Interacting with Ions in Bulk Water. *Struct. Chem.* **2020**, *31*, 975–982.
(51) Lewis, A.; Bumpus, J. A.; Truhlar, D. G.; Cramer, C. J. Molecular Modeling of Environmentally Important Processes: Reduction Potentials. *J. Chem. Educ.* **2004**, *81*, 596–604.
(52) Pittman, K. M.; McAlexander, H. R.; Tschumper, G. S.; Shukla, M. K. Computational Investigation on Electronic Structures and Properties of 4,6-Bis(Nitroimino)-1,3,5-Triazanin-2-One: An Insensitive Munition Compound. *J. Phys. Chem. A* **2019**, *123*, 3504–3509.
(53) Roe, D. R.; Cheatham, T. I. PTRAJ and CPPTRAJ: Software for Processing and Analysis of Molecular Dynamics Trajectory Data. *J. Chem. Theory Comput.* **2013**, *9*, 3084–3095.
(54) Hummer, G.; Pratt, L. R.; Garcia, A. E. Hydration Free Energy of Water. *J. Phys. Chem.* **1995**, *99*, 14188–14194.
(55) Bennett, C. H. Efficient Estimation of the Free Energy Differences from Monte Carlo Data. *J. Comput. Phys.* **1976**, *22*, 245–268.
(56) Takahashi, H.; Suzuoka, D.; Morita, A. Why Is Benzene Soluble in Water?

Role of OH/π Interaction in Solvation. *J. Theor. Comput.* **2015**, *11*, 1181–1194.

(57) Huang, J.; Kingsbury, S.; Kertesz, M. Crystal Packing of TCNQ Anion π-Radicals Governed by Intermolecular Covalent π–π Bonding: DFT Calculations and Statistical Analysis of Crystal Structures. *PCCP* **2008**, *10*, 2625–2635.

REPORT DOCUMENTATION PAGE

Form Approved
OMB No. 0704-0188

1. REPORT DATE *(DD-MM-YYYY)*	2. REPORT TYPE	3. DATES COVERED *(From - To)*
February 2021	Final	

4. TITLE AND SUBTITLE

Computational Investigation on Interactions between Some Munitions Compounds and Humic Substances

5a. CONTRACT NUMBER

5b. GRANT NUMBER

5c. PROGRAM ELEMENT NUMBER
63728

6. AUTHOR(S)

Timothy C. Schutt and Manoj K. Shukla

5d. PROJECT NUMBER
03E

5e. TASK NUMBER
01

5f. WORK UNIT NUMBER

7. PERFORMING ORGANIZATION NAME(S) AND ADDRESS(ES)

U.S. Army Engineer Research and Development Center
Environmental Laboratory
3909 Halls Ferry Road
Vicksburg, MS 39180

8. PERFORMING ORGANIZATION REPORT NUMBER

ERDC/EL MP-21-1

9. SPONSORING / MONITORING AGENCY NAME(S) AND ADDRESS(ES)

US Army Corps of Engineers
Washington, DC 20314-1000

10. SPONSOR/MONITOR'S ACRONYM(S)

11. SPONSOR/MONITOR'S REPORT NUMBER(S)

12. DISTRIBUTION / AVAILABILITY STATEMENT

Approved for public release; distribution is unlimited.

13. SUPPLEMENTARY NOTES

This paper was originally published in the *Journal of Physical Chemistry A* on 14 December 2020. Funding was under USACE Environmental Quality Technology Program and the DoD Environmental Security Technology Certification Program.

14. ABSTRACT

Humic acid substances (HAs) in natural soil and sediment environments effect the retention and degradation of insensitive munitions compounds and legacy high explosives (MCs): DNAN, DNi- NH_4^+, nMNA, NQ, NTO (neutral and anionic forms), TNT, and RDX. A humic acid model compound has been considered using molecular dynamics, thermodynamic integration, and density functional theory to characterize the munition binding ability, ionization potential, and electron affinity compared to that in the water solution. Humic acids bind most compounds and act as both a sink and source for electrons. Ionization potentials suggest HAs are more susceptible to oxidation than the MCs studied. The electron affinity of HAs are very conformation-dependent and spans the same range as the munition compounds. When HAs and MCs are complexed the HAs tend to radicalize first thus buffering MCs against reductive as well as oxidative attacks.

15. SUBJECT TERMS

Munitions compounds, humic acid, MD simulation, DFT investigation, ionization potential, electron affinity

16. SECURITY CLASSIFICATION OF:			17. LIMITATION OF ABSTRACT	18. NUMBER OF PAGES	19a. NAME OF RESPONSIBLE PERSON
a. REPORT	b. ABSTRACT	c. THIS PAGE			19b. TELEPHONE NUMBER *(include area code)*
Unclassified	Unclassified	Unclassified	SAR	33	